

# Linear and Nonlinear Optical Properties of Graphene Quantum Dots: A Computational Study.

Sharma SRKC Yamijala<sup>1</sup>, Madhuri Mukhopadhyay<sup>2</sup>, and Swapan K Pati <sup>\*2,3,\*</sup>

<sup>1</sup>Chemistry and Physics of Materials Unit, Jawaharlal Nehru Centre for Advanced Scientific Research, Bangalore 560064, India.

<sup>2</sup>Theoretical Sciences Unit, Jawaharlal Nehru Centre for Advanced Scientific Research, Bangalore 560064, India.

<sup>3</sup>New Chemistry Unit, Jawaharlal Nehru Centre for Advanced Scientific Research, Bangalore 560064, India.

\*Corresponding author

## Abstract

Due to the advantage of tunability via size, shape, doping and relatively low level of loss and high extent of spatial confinement, graphene quantum dots (GQDs) are emerging as an effective way to control light by molecular engineering. The collective excitation in GQDs shows both high energy plasmon frequency along with frequencies in the terahertz (THz) region making these systems powerful materials for photonic technologies. Here, we report a systematic study of the linear and nonlinear optical properties of large varieties of GQDs ( $\sim 400$  systems) in size and topology utilizing the strengths of both semiempirical and first-principles methods. Our detailed study shows how the spectral shift and trends in the optical nonlinearity of GQDs depends on their structure, size and shape. Among the circular, triangular, stripe, and random shaped GQDs, we find that GQDs with inequivalent sublattice atoms always possess lower HOMO-LUMO gap, broadband absorption and high nonlinear optical coefficients. Also, we find that for majority of the GQDs with interesting linear and nonlinear optical properties have zigzag edges, although reverse is not always true. We strongly believe that our findings can act as guidelines to design GQDs in optical parametric oscillators, higher harmonic generators and optical modulators.

Keywords: ZINDO/S, Polyaromatic hydrocarbons (PAHs), Graphene, Clar's rule, Lieb's theorem.

---

\*pati@jncasr.ac.in

# 1 Introduction

Materials with broadband absorption (BBA) and emission, that is, covering ultraviolet, visible, and near-infrared regions of the solar spectrum, have important applications in photodetectors, broadband modulators, bioimaging, solar cells and so forth.<sup>1-6</sup> Moreover, if the materials with the broadband absorption also shows optical nonlinearity they can be very useful in applications involving optical parametric oscillation, high harmonic generation,<sup>7,8</sup> Kerr effect<sup>9,10</sup> and multiphoton imaging.<sup>11</sup> Thus, finding novel materials with both broadband absorption and optical nonlinear activity is of great interest.

Group IV-VI quantum dots like CdSe, PbSe, CdS, HgTe, ZnSe, etc. have already been there in variety of applications involving light emitting diodes, bio-imaging, solar cells, and so forth, because of their tunable absorption and specific optical nonlinear activity.<sup>12-17</sup> Materials prepared from high band gap semiconductors like ZnS, ZnSe, GaN, and AlN possess ultraviolet optical activity whereas CdS, rare earth doped GaN materials exhibit near IR activities.<sup>18,19</sup> Although, tuning the size of a quantum dot can vary its active optical range, it cannot give the whole range altogether (i.e. simultaneously UV-VIS and IR range activity). To this end, GQDs and modified GQDs seems to be promising materials for such optical activities.<sup>20,21</sup> Together with their higher photostability, bio-compatibility and low cost preparation, GQDs may act as a substitute for the toxic IV-VI group quantum dots.

GQDs are the confined graphene materials available in various topologies<sup>21-23</sup> and graphene is a layered  $sp^2$ -bonded carbon material in honeycomb lattice. Graphene with its zero band gap has a limitation to its applications in optoelectronics due to its zero optical emission. On the other hand, GQDs exhibit a broadband absorption and they have emerged as attractive fluorescence materials in the ultraviolet, visible and even in infrared regions.<sup>20,21,24</sup> During recent years, there has been a lot of research on the broadband activity of GQDs of different sizes, shapes and functionalities through both experiment and theory.<sup>25-28</sup> Also, there is a progress in identifying the shape and size dependent nonlinear activity of GQDs.<sup>29-32</sup>

Considering these studies into account, here, we have performed a systematic computational study on the linear and nonlinear optical (NLO) properties of hydrogen passivated GQDs (hence, may also be termed as polyaromatic hydrocarbons (PAHs)) of various sizes, shapes, edge structures and so forth. After careful analysis on these GQDs ( $\sim 20$ ) with simultaneous BBA and high NLO coefficients, we find that the necessary and sufficient condition for possessing such multifunctionality is the presence of inequivalent sublattice atoms. Also, we find that majority of the GQDs with only zigzag edges possess this multifunctionality. Additionally, we find that some of these GQDs show fascinating 1st hyperpolarizabilities ( $\sim 10^3$ - $10^5$  times larger than the traditional NLO compounds [like p-nitroaniline etc]). In the following, first we have described how we have modeled our systems and then we have given the details of our computations. Next, we have compared the results from our semiempirical calculations on structural stability and electronic properties with the earlier studies and then we have presented our results on linear and nonlinear optical properties. Finally, we have presented the results from first principles calculations on the systems, followed by the conclusions and possible extensions to the present work.

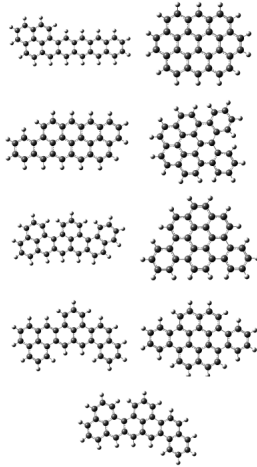


Figure 1: Some random shaped GQDs with 32 carbon atoms (C32)

## 2 Modeling and Computational Details

As the number of varieties of GQDs which can be generated from graphene are huge, following Kuc et. al.<sup>23</sup> we have considered  $\sim 400$  structures, based on their size, shape, edge etc. As the hydrogen passivated GQDs have been shown to be more stable than the GQDs with bare edges, we have only considered the former ones throughout our study. As in ref,<sup>23</sup> we have categorized our GQDs as circular (F) or triangular (T) or stripes (i.e. nanoribbons) (S) depending on their shape and zigzag (z) or armchair (a) depending on their edges. Thus,  $F_a$  ( $T_z$ ) represents circular (triangular) GQDs with armchair (zigzag) edges. All other GQDs which don't fit in these categories mainly represent the different possible conformers of a GQD with particular number of carbon atoms and we refer them as random shaped GQDs. We identify these random shaped GQDs with their carbon atom numbers such as C22, C28, C74 etc. In Figure 1 we have shown typical examples of random shaped GQDs.

All the structural optimizations have been performed using self-consistent charge (SCC) density functional tight-binding (DFTB) theory<sup>33</sup> within third order expansion of the energy (DFTB3)<sup>34</sup> and with 3ob parameter set,<sup>35</sup> as implemented in DFTB+ package.<sup>36</sup> DFTB level of theory is used mainly due to the large number of systems ( $\sim 400$ ) considered in this study as well as its ability to give trends in band-gaps, energies etc. which are comparable to the ones given by DFT, especially for carbon related materials, even with different edges, defects and so forth.<sup>37,38</sup> Geometry optimizations have been performed using conjugate gradient method and systems are considered to be optimized only when forces on all the atoms are less than 0.0001 Ha/Bohr. As the systems are zero-dimensional, we have performed the  $\Gamma$ -point calculations. For those systems whose energy levels near the Fermi-level are almost degenerate, we have increased the electronic temperature to 100 K to avoid any convergence issues.

Linear optical properties of all the compounds have been computed at the semi-empirical ZINDO/S level of theory as implemented in g09 software package.<sup>39</sup>

ZINDO/S has been proved to be very successful especially in predicting the optical properties of systems containing C, N, O, H atoms like polyaromatic hydrocarbon compounds,<sup>40,41</sup> chlorophylls<sup>42</sup> etc.<sup>43</sup> At semi-empirical level, nonlinear optical (NLO) properties of all compounds have been calculated using MOPAC 2012 program package.<sup>44,45</sup> All the first principles calculations for the linear (at time dependent density functional theory (TDDFT) level) and nonlinear optical properties have been performed using g09. Long range corrected (CAM-B3LYP) exchange correlation functional has been used in conjunction with 6-31+g(d) basis set for all the calculations. A minimum of first 12 lowest excited states have been considered in all the studies. GaussSum-2.2.6.1<sup>46</sup> is used to plot the absorption spectra and a broadening of 0.333 eV has been used. To ensure the reliability of our calculations, we have compared our semi-empirical and first principles results on the linear and nonlinear optical properties of p-nitroaniline with its reported experimental values. We find that both the results are in close agreement (see Table S1 of supporting information (SI)).

### 3 Results and Discussion

#### 3.1 Energetic Stability and Electronic Properties:

All the GQDs considered in this study are found to be thermodynamically stable, that is, they have negative formation energy,  $E_{Form} = E_{tot} - N_H * E_H - N_C * E_C$ , where  $E_{tot}$ ,  $E_H$  and  $E_C$  are the total energy of the system, energy of the hydrogen atom in a  $H_2$  molecule (i.e.  $E_{H2}/2$ ) and energy of the carbon atom in a graphene lattice (i.e.  $E_{Graph}/N_C$ ), respectively. Here,  $N_C$  and  $N_H$  are the number of carbon and hydrogen atoms in the system. At DFTB3 level of theory, we find  $E_H$  and  $E_C$  to be -9.123 and -44.291 eV, respectively. A plot of formation energy per atom vs  $N_H/(N_H+N_C)$  of all the systems is given in Fig. 2a. Clearly, there is a near linear relationship between the formation energy per atom and the number of edge atoms in all the systems (notice the linear fit in Fig. 2a), that is, system with lesser number of edge atoms is easier to form and vice-versa, as expected.<sup>20,47,48</sup> Similar results have been observed in some of the earlier studies on GQDs and PAHs<sup>23,49</sup> In agreement with these previous studies, we also find that among the different GQD shapes studied here, circular GQDs are the most stable ones and ribbon like GQDs are the least stable. All other GQDs' (triangular, random etc.) stability fall in between these two types of GQDs [see Fig. 2a]. The reason for such a trend is again due to the less number of edge atoms in circular GQDs than in other GQDs considered in this study, as evident from the x-axis of Fig. 2a. Recent molecular dynamics simulations have also shown that among the different GQDs, circular and triangular GQDs with zigzag edges as the most stable ones till  $\sim 4000$  K.<sup>22</sup>

Next, the energies of HOMO, LUMO and their difference (i.e. HOMO-LUMO gap (HLG)) of all the GQDs are plotted in Fig. 2b as a function of number of carbon atoms. The calculated HLG values are mainly in the range of  $\sim 0-3$  eV. Also, from Fig. 2b and 2c, it can be observed that for a particular  $N_C$ , one can tune the HLG from  $\sim 0-3$  eV depending on the shape and edges of the GQD. Also it should be noted that such tuning is possible even for the systems with  $N_C$  between 20 to 50. In fact, synthesis of GQDs (actually, PAHs) of different sizes have already been carried out.<sup>21</sup> From Fig. 2c, it can be noticed that

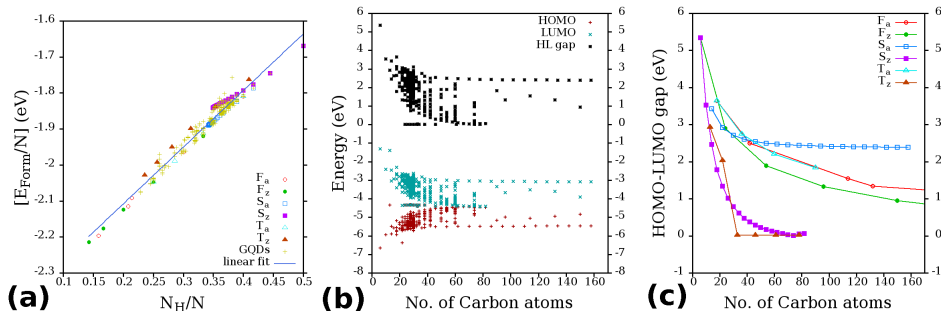


Figure 2: (a) A plot of  $E_{Form}$  per atom versus number of edge atoms to the total number of atoms ( $N$ ) of all the GQDs. Straight line shows the linear fit. (b) Energies of HOMO, LUMO and the HOMO-LUMO gap (HLG) of all the GQDs and (c) Changes in the HLG with size for different shaped GQDs. Symbols T, F, S represents triangular, circular and striped GQDs. Subscripts a and z represents armchair and zigzag edges. See the “Modeling” for further details.

HLG of the systems with zigzag edges converge rapidly to zero (reaching the semi-metallicity of graphene) than the armchair ones, irrespective of the shapes and the calculated trend of convergence is  $T_z$ -GQDs >  $S_z$ -GQDs >  $F_z$ -GQDs >  $T_a$ -GQDs  $\sim$   $F_a$ -GQDs >  $S_a$ -GQDs. As HLG reflects the kinetic stability of a system, the above trends suggest that kinetic stability will be highest for  $S_a$ -GQDs and least for  $T_z$ -GQDs and  $S_z$ -GQDs. As suggested by the Clars rule,<sup>21</sup> higher kinetic stability of  $S_a$ -GQDs, compared to the other structures is due to the presence of larger number resonant sextets in these structures. Similar reasons are also known for the lesser stability of zigzag edged structures compared to the armchair ones.<sup>23</sup> One may also notice that the HLG of “ $S_z$  and  $T_z$ ”, “ $T_a$  and  $F_a$ ”-GQDs follows similar trend as  $N_C$  increases (for  $N_C > 60$ ) as has also been observed in some of the recent studies.<sup>22</sup> Finally, as the HLG of these GQDs are tunable over a wide range and as HLG can be used as a rough estimate for the optical gap,<sup>40</sup> one may immediately expect that the optical properties of these GQDs can also be tuned over a wide range and the results of the respective calculations are given below.

### 3.2 Optical Properties:

First, we present the optical absorption of all the systems calculated at the ZINDO/S level of theory. Here, we have analyzed only the 20 low energy singlet excitations from the ZINDO/S results. Absorption spectra of PAHs mainly consists of 3 bands, namely, alpha ( $\alpha$ ), beta ( $\beta$ ) and para ( $p$ ), out of which the most intense ones being  $\beta$  and  $p$ -bands (notations are according to Clar’s rule,<sup>21</sup> where  $p(\beta)$ -bands corresponds to the bands at higher (lower) wavelengths). Interestingly, in a very recent study<sup>40</sup> it has been concluded that ZINDO/S is good at predicting the most intense  $p$  and  $\beta$  bands of all  $C_{32}H_{16}$  benzenoid PAHs. Considering these facts, first we have plotted the histograms of “wavelengths corresponding to the most intense  $p$ -bands ( $p_{max}$ ) and  $\beta$ -bands ( $\beta_{max}$ )”, respectively, in Figs. 3a and 3b and the corresponding oscillator strengths (OS) histograms in Figs. S1a and S1b. From these figures

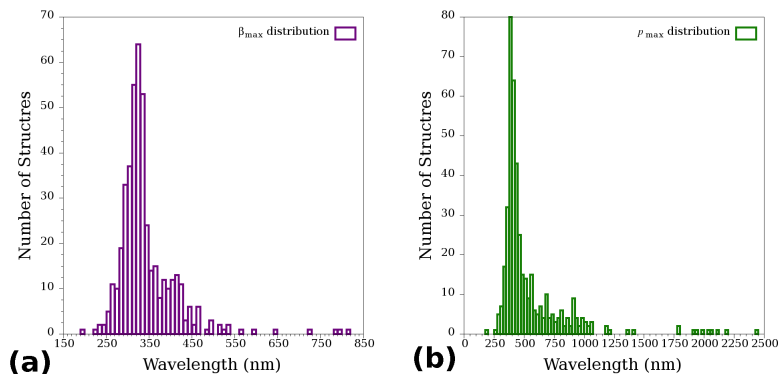


Figure 3: Histograms of wavelengths corresponding to (a)  $\beta_{max}$ , (b)  $p_{max}$  excitation in all GQDs.  $p_{max}$  excitations above 2500 nm have been omitted for clarity.

it can be noticed that, majority of the systems have their  $\beta_{max}$  and  $p_{max}$  in the UV-VIS region (200-760 nm) and the oscillator strength of  $\beta_{max}$  ( $p_{max}$ ) is almost always (for majority of structures)  $> 0.5$  ( $0.1$ ). Thus, majority of GQDs considered in this study absorb strongly in the UV-VIS region (in particular, their  $\beta_{max}$  ( $p_{max}$ ) is located in the region between 250-450 (300-700) nm).

However, interestingly, we find  $\sim 70$  GQDs whose  $p_{max}$  is in IR-region ( $> 760$  nm). Materials absorbing in IR region are of great interest in the preparation of solar cells because half of the solar energy received by earth is in IR radiation range and most of the present day solar cells do not utilize this energy region.<sup>20</sup> Thus, knowing the reason for the IR-activity of these GQDs will be of great use and for this we have analyzed their  $p_{max}$  transition. In Table S1, we have given the calculated wavelength, OS and the major contributions of the molecular orbitals corresponding to the  $p_{max}$  transition for all the IR-active GQDs. Clearly,  $p_{max}$  transition always has the major contributions from excitations involving the frontier orbitals (that is, HOMO-1, HOMO, LUMO and LUMO+1), especially from HOMO and LUMO. Thus, the changes in these frontier MOs lead to changes in the  $p_{max}$  transition. Also, some of the earlier studies on PAHs have found that HLG of these systems is almost equal to the energy corresponding to the  $p_{max}$  transition (see Ref<sup>40</sup> and references there in).

For a few of these GQDs, we find HLG to be very small. In general, small HLGs occur either due to extended delocalization (as in conjugated carbon chains) or if there exists lesser number of resonant sextets (according to Clar's rule<sup>21,23,40</sup>). In our case, however, the very small HLGs are seen due to completely different reasons. If we look at the structures of these GQDs closely, we find that, they don't have same number of sublattice atoms (i.e.  $N_A - N_B \neq 0$ ). In fact, in all the random shaped GQDs, we find there exists two additional sublattice atoms of one type (i.e.  $|N_A - N_B| = 2$ ).  $p_z$  orbitals of these additional atoms remains as non-bonding orbitals and appear at the zero of energy (i.e. at the Fermi-level) in the energy level diagram. If there were no interactions (as in tight-binding calculations), both of these levels would be degenerate and would appear exactly at the zero of energy. (similar to what has been observed in triangular GQDs<sup>50</sup>). However, because of interaction terms in

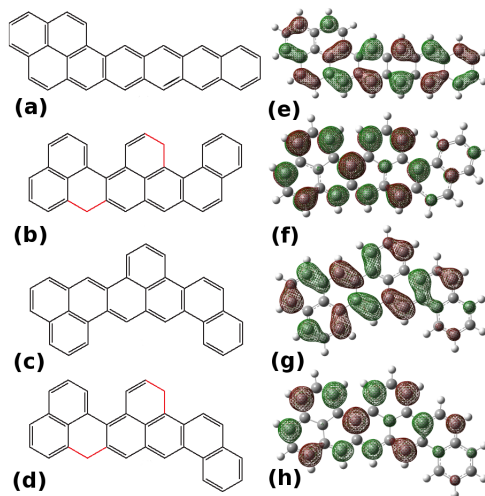


Figure 4: Schematic diagrams of four structural isomers of  $C_{32}H_{18}$  GQD are given in (a)-(d) and their HOMO isosurfaces are given in (e)-(h), respectively. Iso-value of  $0.02 \text{ e}/\text{\AA}^3$  is used for all the plots.

ZINDO/S Hamiltonian, we find the two levels to appear above and below the zero of energy with a very low energy gap (few meV). Interestingly, these two levels have opposite parity, due to which the transition dipole moment between the two become non-zero. Thus, these two levels give rise to optical transition with a finite oscillator strength (OS). Since, the energy gap between these two levels is too small, the optical absorption appears in IR-region.

As an example, in Figs. 4a-4d we have given four structural isomers (here after, addressed as 4a, 4b, 4c and 4d, respectively) of  $C_{32}H_{18}$ , where only 4b and 4d have the sublattice imbalance. As explained, only for 4b and 4d, we find  $p_{max}$  in IR-region ( $> 2000 \text{ nm}$ ) but not for 4a and 4c. In Fig. 4, we have also given the conjugation and isosurface plots of HOMO for these GQDs. As can be seen, because of sublattice imbalance, the conjugation in 4b and 4d GQDs is not continuous and there are “conjugation breaks”, which are clear demonstration of solitonic structure (conjugated system), domain walls (seen in ferromagnetic metal blocks). The main point is that, these defect states are intrinsic in these GQDs and these have not been externally induced.

IR-activity of GQDs which absorb below  $2500 \text{ nm}$  is mainly due to the zigzag edge nature of these GQDs, which lowers their HLG. For example, it is well known that the polyacenes have the lowest HLG among the various PAHs<sup>21</sup> and  $p_{max}$  of hexacene (6 fused benzene rings) itself is  $750 \text{ nm}$ . Also, through TDDFT calculations, previously our group has shown that  $p_{max}$  of rectangular GQDs is  $\sim 1900 \text{ nm}$ .<sup>20</sup> Inspecting the structures of GQDs which absorb in the region of  $760\text{-}2500 \text{ nm}$ , we find that all these GQDs have either polyacene type structure or rectangular type structure, with some of their edges being substituted with ethene, propene, cis-1,3-dibutene etc. (see Fig. S3) Also, it is important to mention that HOMO of all the IR-active structures is different from that of the non-IR-active structures.

Frontier MOs of IR-active GQDs have larger number of nodes, and hence, look like the collection of  $p_z$  orbitals on individual carbon atoms without overlap

(for example, see Figs. 4f and 4h). The reverse is true for the non-IR-active GQDs (see Figs. 4e, 4g). Presence of large number of nodes destabilizes HOMO compared to its structural isomers with less number of nodes, and hence, lesser HLG and IR-activity. As an example of the above mentioned observations, we have given absorption spectra and isosurfaces of HOMO of C32 and C74 GQDs in Figs. S2-S4. Finally, as the OS of  $p_{max}$  peak for majority of these GQDs is  $> 0.5$  and as OS of  $\beta_{max}$  peak is almost always found to  $> 0.5$ , we find that these GQDs can have broad band absorption (BBA), as predicted earlier for the rectangular GQDs.<sup>20</sup> BBA of these GQDs can also be seen in Figs. S2 and S4. To conclude all the above results, we find that GQDs with inequivalent sublattice atoms or GQDs with rectangular or stripe shapes can absorb in IR-region and they may be suitable candidates for BBA.

To put the results obtained from the ZINDO/S method in a solid footing, we have performed TDDFT calculations at CAMB3LYP/6-31+g(d) level of theory on a few GQDs. First, we will present our results on GQDs of various shapes. In Figs. 5a-5f, we have given the absorption spectra of  $S_a$ ,  $S_z$ ,  $F_a$ ,  $F_z$ ,  $T_a$  and  $T_z$ , respectively, calculated at both ZINDO/S and TDDFT levels of theory along with the iso-surfaces of their HOMO (only from TDDFT). Clearly, absorption profiles of both the methods compares fairly well, although OS values predicted by ZINDO/S are higher than that of TDDFT. Also,  $\lambda_{max}$  predicted by ZINDO/S is consistently red-shifted compared to the TDDFT predicted values. Consistent with the previous arguments on the isosurface of HOMO (calculated using ZINDO/S), even with TDDFT we find larger number of nodes (see Fig. 5f) in the HOMO if the GQD has IR-activity and it has more overlapping character if the GQD is not IR-active (see Fig. 5a-5e). Also, we find that the character of the  $p_{max}$  excitation (i.e. MOs involved in the excitation) are similar in both the methods. Importantly, we find that GQDs whose HOMO is mainly localized on the edge atoms (as in  $S_z$  and  $T_z$ ) and whose  $p_{max}$  excitation has major contribution from HOMO to LUMO, are IR-active. From Fig. 5, one may also infer that the presence of zigzag edges is only a necessary, but not a sufficient condition (example being the  $F_z$  GQDs) for the IR-absorption. Finally, to see the effect of inequivalent sublattice atoms on the IR-activity, we have considered five C28-GQDs with  $N_A - N_B = 2$ , and we find all of them to be IR active, again consistent with the ZINDO/S results (see Table S2). Thus, we find that, results of ZINDO/S and TDDFT are consistent and compare well for the GQDs considered in this study.

### 3.3 Nonlinear Optical Properties:

In this subsection, we present the linear polarizability ( $\alpha$ ) and first hyperpolarizability ( $\beta$ ) of all the GQDs calculated using the finite field approach as implemented in the MOPAC and g09 packages. Expressions for the dipole moment and the energy of a molecule interacting with an external electric field are given by Eqns. 1 and 2.<sup>51</sup>

$$\mu_i = \mu_0 + \alpha_{ij}F_j + \frac{1}{2}\beta_{ijk}F_jF_k + \frac{1}{6}\gamma_{ijkl}F_jF_kF_l + \dots \quad (1)$$

$$E(F) = E(0) - \mu_iF_i - \frac{1}{2!}\alpha_{ij}F_iF_j - \frac{1}{3!}\beta_{ijk}F_jF_k - \frac{1}{4!}\gamma_{ijkl}F_jF_kF_l - \dots \quad (2)$$



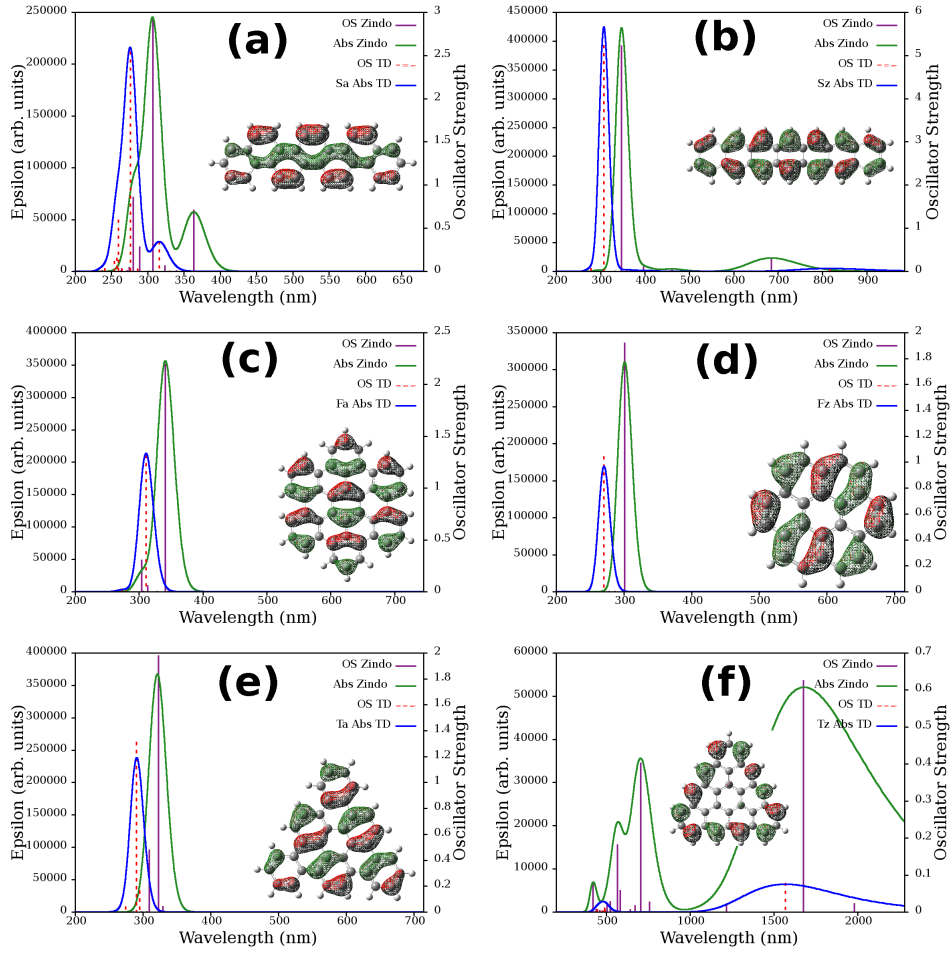


Figure 5: Absorption profiles of GQDs of various shapes calculated at both ZINDO/S level of theory and using TDDFT at CAMB3LYP/6-31+g(d) level of theory. Insets in each figure show the isosurface of the HOMO of that GQD calculated using TDDFT. (a)-(f) represents  $S_a$ ,  $S_z$ ,  $F_a$ ,  $F_z$ ,  $T_a$  and  $T_z$  GQDs, respectively. Iso-value of  $0.02 \text{ e}/\text{\AA}^3$  is used for all the plots.

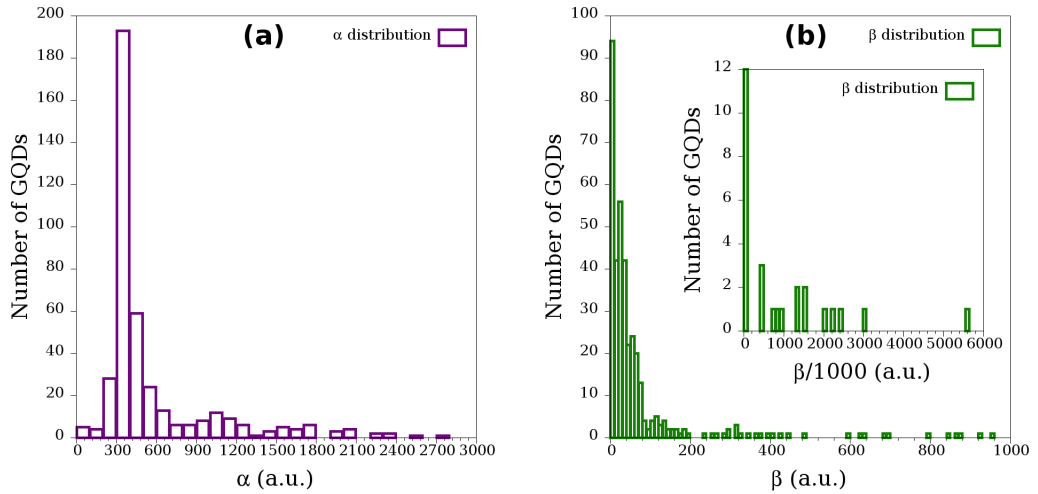


Figure 6: Histograms of average values of (a) polarizability,  $\alpha$  and (b) first hyperpolarizability,  $\beta$  of all GQDs.

where,  $\mu_0$  is the permanent dipole moment,  $\alpha_{ij}$ ,  $\beta_{ijk}$  and  $\gamma_{ijkl}$  are the linear polarizability, 1<sup>st</sup> and 2<sup>nd</sup> hyperpolarizability tensor elements, respectively. Also, for a molecule, the average values of above quantities ( $\mu_{av}$  etc.) are defined as

$$\mu_{av} = (\mu_x^2 + \mu_y^2 + \mu_z^2)^{1/2} \quad (3)$$

$$\alpha_{av} = \frac{1}{3}(\alpha_{xx} + \alpha_{yy} + \alpha_{zz}) \quad (4)$$

$$\beta_{av} = (\beta_x^2 + \beta_y^2 + \beta_z^2)^{1/2} \quad (5)$$

where,

$$\beta_i = \frac{3}{5}(\beta_{iii} + \beta_{ijj} + \beta_{ikk}), i, j, k = x, y, z \quad (6)$$

In Figs. 6a and 6b, we have plotted the distribution of average  $\alpha$  and  $\beta$  values for all the GQDs at static field. Similar to absorption profiles, majority of the GQDs'  $\alpha$  and  $\beta$  values are confined to a small region. For these majority GQDs, we find that the  $\alpha$  and  $\beta$  values are in the range of 250–700 a.u. ( $\sim 40$ – $100 \text{ \AA}^3$ ) and 1–200 a.u. ( $10^{-32}$ – $10^{-30}$  esu), respectively. Compared to the  $\alpha$  and  $\beta$  values of para-nitroaniline (16.346 a.u. and 978.21 a.u., respectively), it is nice to notice that majority of the GQDs already have high polarizability and reasonable hyperpolarizabilities. Importantly, we find that several GQDs possess  $\alpha$  and  $\beta$  values which are orders of magnitude greater than that of para-nitroaniline (see Fig 6a and inset of Fig 6b).

In general, both linear polarizability and first order hyperpolarizabilities have an inverse relationship with the energy gap between the states involved in the polarization, and are directly proportional to the transition moment. Thus, we can expect an increase in  $\alpha$  and  $\beta$  if the ground and excited states are closely spaced or the transition moment between the states is high or both. From the above reasoning, one can also infer that GQDs with low HLG and whose 1<sup>st</sup> excited state has major contribution from HOMO to LUMO transition should

give higher  $\alpha$  and  $\beta$  values. Indeed, we find that all the GQDs which are IR-active also have high  $\alpha$  and  $\beta$  (except the GQDs with inversion symmetry) values, that is, above the range of 250–700 a.u. and 1–200 a.u., respectively. Also, we find that some of the GQDs with zigzag edges, like  $F_z$ , which are not IR-active but have very high oscillator strength for the  $p_{max}$  (see Fig. 5d) excitation also show higher  $\alpha$  values. However, to the presence of inversion symmetry, such GQDs do not have higher  $\beta$  values. Finally, we again find that trends in our results from semiempirical calculations compares fairly well with that of first-principle calculations (see Table S4). Based on all the above results, we conjecture that GQDs with very low HLGs can have both broad band absorption and nonlinear optical activity, and hence, are potential candidates for optoelectronic devices.

## 4 Conclusions

We have performed a systematic study on the GQDs of various sizes, shapes and edges to explore their linear and nonlinear optical properties. First, we find the formation energies of GQDs have a near linear dependence on their number of edge atoms and HOMO-LUMO gaps of a GQD with a particular number of carbon atoms can be tuned from  $\sim 0$ -3 eV depending on its shape and edge nature. Trends in the HLG can be understood based on the Clar’s rule of aromatic sextets for majority of the systems. Extremely low HLGs of certain GQDs is due to the presence of unequal number of sublattice atoms in these GQDs, that is,  $N_A - N_B \neq 0$ . Tunability of HLG has also been reflected in the tunability of the absorption profiles in these GQDs. We find that majority of the GQDs absorb strongly in the UV-VIS region with their  $\beta_{max}$  ( $p_{max}$ ) being located in the region between 250-450 (300-700) nm and their  $\alpha$  and  $\beta$  values are in the range of 250–700 a.u. and 1–200 a.u., respectively. However,  $\sim 70$  GQDs have their  $p_{max}$  in IR-region and have higher  $\alpha$  ( $> 700$  a.u.) and  $\beta$  ( $> 200$  a.u.) values. A common feature which we find in all these IR-active GQDs is the existence of larger number of nodes in the isosurface of HOMO which leads to an increment in HOMO energy, and hence, decrement in the HLG. Due to their high oscillator strengths in both UV-VIS and IR-regions these GQDs can possess broad band absorption. With their high  $\alpha$  and  $\beta$  values along with the BBA, we expect them to be potential candidates for optoelectronic devices.

## References

- [1] Zheng, J.; Barton, R. a.; Englund, D. *ACS Photonics* **2014**, *1*, 768–774.
- [2] Sun, H.; Autschbach, J. *Journal of Chemical Theory and Computation* **2014**, *10*, 1035–1047.
- [3] Kim, J. T.; Yu, Y.-J.; Choi, H.; Choi, C.-G. *Optics express* **2014**, *22*, 803–8.
- [4] Sobon, G.; Sotor, J.; Pasternak, I.; Strupinski, W.; Krzempek, K.; Kaczmarek, P.; Abramski, K. M. *Laser Physics Letters* **2013**, *10*, 035104.
- [5] Urich, A.; Unterrainer, K.; Mueller, T. *Nano letters* **2011**, *11*, 2804–8.

- [6] Sun, Z.; Hasan, T.; Torrisi, F.; Popa, D.; Privitera, G.; Wang, F.; Bonaccorso, F.; Basko, D. M.; Ferrari, A. C. *ACS nano* **2010**, *4*, 803–10.
- [7] Sø rngård, S. A.; Simonsen, S. I.; Hansen, J. P. *Physical Review A* **2013**, *87*, 053803.
- [8] Hong, S.-Y.; Dadap, J. I.; Petrone, N.; Yeh, P.-C.; Hone, J.; Osgood, R. M. *Physical Review X* **2013**, *3*, 021014.
- [9] Shen, T.-Z.; Hong, S.-H.; Song, J.-K. *Nature materials* **2014**, *13*, 394–9.
- [10] Shimano, R.; Yumoto, G.; Yoo, J. Y.; Matsunaga, R.; Tanabe, S.; Hibino, H.; Morimoto, T.; Aoki, H. *Nature communications* **2013**, *4*, 1841.
- [11] Yang, H.; Feng, X.; Wang, Q.; Huang, H.; Chen, W.; Wee, A. T. S.; Ji, W. *Nano letters* **2011**, *11*, 2622–7.
- [12] Mashford, B. S.; Stevenson, M.; Popovic, Z.; Hamilton, C.; Zhou, Z.; Breen, C.; Steckel, J.; Bulovic, V.; Bawendi, M.; Coe-Sullivan, S.; Kazlas, P. T. *Nature Photonics* **2013**, *7*, 407–412.
- [13] Klimov, V.; Mikhailovsky, A.; Xu, S. *Science* **2000**, *290*, 314–318.
- [14] Choi, H.; Radich, J. G.; Kamat, P. V. *The Journal of Physical Chemistry C* **2014**, *118*, 206–213.
- [15] Tian, J.; Liu, R.; Zhao, Y.; Peng, Y.; Hong, X.; Xu, Q.; Zhao, S. *Nanotechnology* **2010**, *21*, 305101.
- [16] Somers, R. C.; Bawendi, M. G.; Nocera, D. G. *Chemical Society reviews* **2007**, *36*, 579–91.
- [17] Lad, A. D.; Prem Kiran, P.; Ravindra Kumar, G.; Mahamuni, S. *Applied Physics Letters* **2007**, *90*, 133113.
- [18] Shavel, A.; Gaponik, N.; Eychmüller, A. *The Journal of Physical Chemistry B* **2004**, *108*, 5905–5908.
- [19] Dennis, A. M.; Mangum, B. D.; Piryatinski, A.; Park, Y.-S.; Hannah, D. C.; Casson, J. L.; Williams, D. J.; Schaller, R. D.; Htoon, H.; Hollingsworth, J. a. *Nano letters* **2012**, *12*, 5545–51.
- [20] Yamijala, S. S.; Pati, S. K. *The Journal of Physical Chemistry C* **2013**, *117*, 3580–3594.
- [21] Rieger, R.; Müllen, K. *Journal of Physical Organic Chemistry* **2010**, *23*, 315–325.
- [22] Silva, a. M.; Pires, M. S.; Freire, V. N.; Albuquerque, E. L.; Azevedo, D. L.; Caetano, E. W. S. *The Journal of Physical Chemistry C* **2010**, *114*, 17472–17485.
- [23] Kuc, a.; Heine, T.; Seifert, G. *Physical Review B* **2010**, *81*, 085430.
- [24] Sk, M. A.; Ananthanarayanan, A.; Huang, L.; Lim, K. H.; Chen, P. *Journal of Materials Chemistry C* **2014**, *2*, 6954.

- [25] Fang, Z.; Wang, Y.; Schlather, A.; Liu, Z. *Nano letters* **2013**, *14*, 299–304.
- [26] Yan, X.; Li, B.; Li, L.-s. *Accounts of chemical research* **2013**, *46*, 2254–62.
- [27] Tang, L.; Ji, R.; Li, X.; Bai, G.; Liu, C. P.; Hao, J.; Lin, J.; Jiang, H.; Teng, K. S.; Yang, Z.; Lau, S. P. *ACS nano* **2014**, *8*, 6312–20.
- [28] Riesen, H.; Wiebeler, C.; Schumacher, S. *The journal of physical chemistry. A* **2014**, *118*, 5189–95.
- [29] Zhou, Z.; Liu, Z.; Li, Z. *The Journal of Physical Chemistry C* **2011**, 16282–16286.
- [30] Yoneda, K.; Nakano, M.; Kishi, R.; Takahashi, H.; Shimizu, A.; Kubo, T.; Kamada, K.; Ohta, K.; Champagne, B.; Botek, E. *Chemical Physics Letters* **2009**, *480*, 278–283.
- [31] Yoneda, K.; Nakano, M.; Fukuda, K.; Champagne, B. *The Journal of Physical Chemistry Letters* **2012**, *3*, 3338–3342.
- [32] Yoneda, K.; Nakano, M.; Inoue, Y. *The Journal of Physical Chemistry C* **2012**, *116*, 17787–17795.
- [33] Elstner, M.; Porezag, D.; Jungnickel, G.; Elsner, J.; Haugk, M.; Frauenheim, T.; Suhai, S.; Seifert, G. *Physical Review B* **1998**, *58*, 7260–7268.
- [34] Yang, Y.; Yu, H.; York, D.; Cui, Q.; Elstner, M. *The journal of physical chemistry. A* **2007**, *111*, 10861–73.
- [35] Gaus, M.; Goez, A.; Elstner, M. *Journal of Chemical Theory and Computation* **2013**, *9*, 338–354.
- [36] Aradi, B.; Hourahine, B.; Frauenheim, T. *The Journal of Physical ...* **2007**, *111*, 5678–84.
- [37] Zobelli, A.; Ivanovskaya, V.; Wagner, P.; Suarez-Martinez, I.; Yaya, A.; Ewels, C. P. *Physica Status Solidi (B)* **2012**, *249*, 276–282.
- [38] Enyashin, A. N.; Ivanovskii, A. L. *Physica Status Solidi (B)* **2011**, *248*, 1879–1883.
- [39] Frisch, M. J. et al. Gaussian09 Revision B.01. Gaussian Inc. Wallingford CT 2009.
- [40] Oña Ruales, J. O.; Ruiz-Morales, Y. *The journal of physical chemistry. A* **2014**, *118*, 5212–27.
- [41] Cocchi, C.; Prezzi, D.; Ruini, A. *The Journal of Physical Chemistry A* **2014**, *118*, 6507–6513.
- [42] Linnanto, J.; Korppi-Tommola, J. *Physical Chemistry Chemical Physics* **2000**, *2*, 4962–4970.
- [43] Voityuk, A. a. *Wiley Interdisciplinary Reviews: Computational Molecular Science* **2013**, *3*, 515–527.

- [44] MOPAC2012, James J. P. Stewart, Stewart Computational Chemistry, Version 14.212L web: [HTTP://OpenMOPAC.net](http://OpenMOPAC.net).
- [45] Maia, J. D. C.; Urquiza Carvalho, G. A.; Manguiera, C. P.; Santana, S. R.; Cabral, L. A. F.; Rocha, G. B. *Journal of Chemical Theory and Computation* **2012**, *8*, 3072–3081.
- [46] O’Boyle, N. M.; Tenderholt, A. L.; Langner, K. M. *Journal of computational chemistry* **2008**, *29*, 839–45.
- [47] Yamijala, S. S.; Bandyopadhyay, A.; Pati, S. K. *Chemical Physics Letters* **2014**, *603*, 28–32.
- [48] Bandyopadhyay, A.; Yamijala, S. S. R. K. C.; Pati, S. K. *Physical chemistry chemical physics : PCCP* **2013**, *15*, 13881–7.
- [49] Fthenakis, Z. G. *Molecular Physics* **2013**, *111*, 3289–3296.
- [50] Fernández-Rossier, J.; Palacios, J. *Physical Review Letters* **2007**, *99*, 177204.
- [51] Kurtz, H. A.; Stewart, J. J. P.; Dieter, K. M. *Journal of computational chemistry* **1990**, *11*, 82–87.

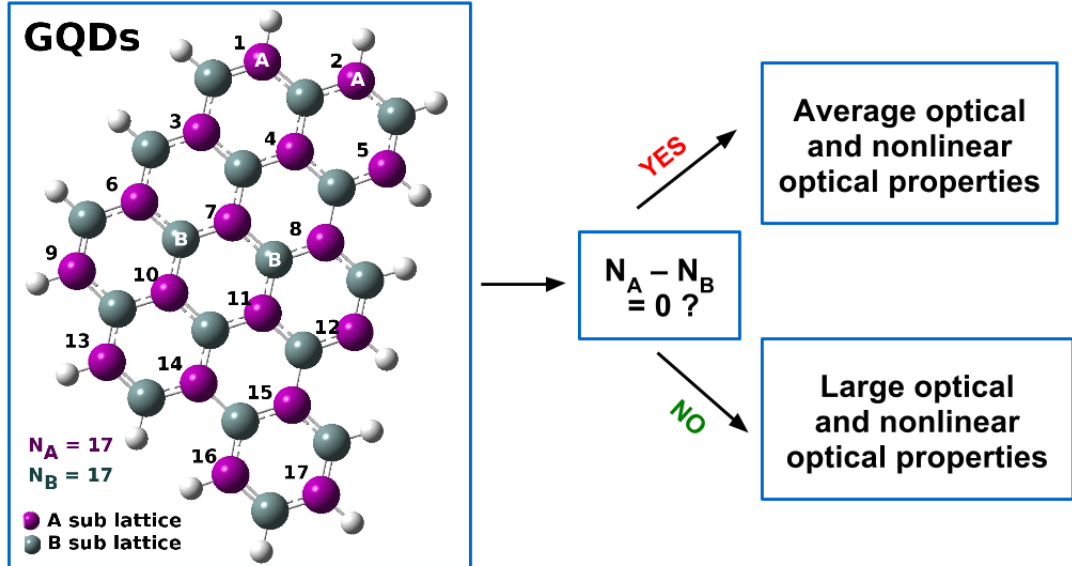
## 5 Supporting Information

Table containing the wavelength, OS and MO contributions to the  $p_{max}$  transition for the GQDs with  $p_{max}$  in IR-region are given. Absorption spectra and isosurfaces of HOMO are given for C32 and C74 GQDs. Comparison of ZINDO/s results with TDDFT and experimental results are also given. This material is available free of charge via the Internet at <http://pubs.acs.org>.

## 6 Acknowledgments

S.S.R.K.C.Y., M. M and S.K.P. acknowledge TUE-CMS, JNCASR for the computational facilities and DST for funding. S.S.R.K.C.Y. thank Dr. Noel for his help in GaussSum.

# Graphical TOC entry



GQDs with nonequivalent number of sublattice atoms show larger linear and nonlinear optical properties.

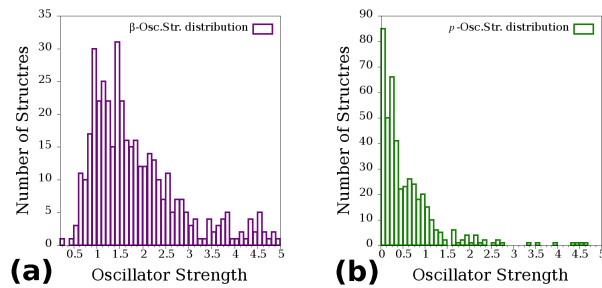


**Figure S1:** Histograms of oscillator strengths corresponding to (a)  $\beta_{max}$ , (b)  $p_{max}$  excitation in all GQDs.

**Table S1:** Reported values of the absorption, polarizability and 1st hyperpolarizability (at static field) for p-nitro aniline along with the results from the present work

Methods	Absorption (nm)	$\alpha_{av}$ (a.u.)	$\beta_{av}$ (a.u.)
Experimental	350 (in dioxane) <sup>a</sup> 375 (in water)	114.7 <sup>b</sup>	1072(+/-44) <sup>c</sup>
DFT reported	291 <sup>d</sup>	102.8 <sup>e</sup>	1794.7 <sup>e</sup> ( $\beta^x$ )
QM/MM	266 <sup>f</sup>	110.3 <sup>g</sup>	978.2 <sup>g</sup>
DFT <sup>h</sup>	269	94.9	3741
Semiempirical <sup>h</sup>	316	100.5	492.5

a) Ultrafast Charge-Transfer Dynamics: Studies of p-Nitroaniline in Water and Dioxane, C. L. Thomsen, J.

Thgersen, and S. R. Keiding J. Phys. Chem. A 1998, 102, 1062-1067.

b) Experimental Investigations of Organic Molecular Nonlinear Optical Polarizabilities. 1. Methods and Results on Benzene and Stilbene Derivatives Ching, L-T.; Tam, W.; Stevenson, S. H.; Meredith, G.; Rikken, G.; Marder, S. R. J Phys Chem 1991, 95, 10631.

c) A comparison of molecular hyperpolarizabilities from gas and liquid phase measurements Kaatz, P.; Donley, E. A.; Shelton, D. P. J Chem Phys 1998,108, 849.

d) Relaxation of Optically Excited p-Nitroaniline: Semiempirical Quantum-Chemical Calculations Compared to Femtosecond Experimental Results, Vadim M. Farztdinov, Roland Schanz, Sergey A. Kovalenko, and Nikolaus P. Ernsting J. Phys. Chem. A 2000, 104, 11486-11496.

e) B3LYP Study of the Dipole Moment and the Static Dipole (Hyper)Polarizabilities of para-Nitroaniline in Gas Phase. Int. J. Quan. Chem. 2006, 106, 11301137.

f) Solvent Effects on the Electronic Transitions of p-Nitroaniline: A QM/EFP Study, Dmytro Kosenkov and Lyudmila V. Slipchenko, J. Phys. Chem. A 2011, 115, 392401.

g)The first hyperpolarizability of p-nitroaniline in 1,4-dioxane: A quantum mechanical/molecular mechanics study, Lasse Jensen, Piet Th. van Duijnen, J. Chem. Phys. 2005, 123, 074307.

h)This work. DFT at CAMB3LYP/6-31+g(d) level of theory. Semiempirical results of absorption are calculated with ZINDO/S and  $\alpha$  and  $\beta$  with MOPAC.



Systems	Wavelength (nm)	Osc. Str.	MO contributions
c38hf	764.6684	0.9090	HOMO→LUMO (93%)
c42hd	781.5389	0.2922	HOMO→LUMO (93%)
c74ha	784.6053	9.4406	HOMO→L+1 (45%), H-1→LUMO (46%)
c60hm	799.0677	1.6014	HOMO→LUMO (91%)
c54he	803.7818	0.8854	HOMO→LUMO (91%)
c78h42	805.0343	0.5534	H-1→L+1 (69%), H-2→L+2 (22%)
c38ha	808.7628	0.3008	HOMO→LUMO (93%)
c60hk	812.7390	1.1520	HOMO→LUMO (93%)
c54hh	823.9738	0.6357	HOMO→LUMO (93%)
c82h44	827.3278	0.5781	H-1→L+1 (66%), H-2→L+2 (25%)
c42hh	827.8249	0.9441	HOMO→LUMO (93%)
c50hd	856.1794	0.9842	HOMO→LUMO (93%)
c54hc	859.8012	0.3036	HOMO→LUMO (91%)
c42hc	860.1591	0.3094	HOMO→LUMO (92%)
c50hb	882.9464	0.3115	HOMO→LUMO (91%)
c60hb	893.8313	0.7016	HOMO→LUMO (82%)
c54hg	900.3873	0.9397	HOMO→LUMO (93%)
c60ho	902.2876	1.7710	HOMO→LUMO (94%)
c60hf	904.4597	0.6102	HOMO→LUMO (92%)
c74hs	905.2522	0.0556	HOMO→L+1 (72%), HOMO→L+5 (11%)
c60hh	908.3694	1.0712	HOMO→LUMO (92%)
c60hp	910.4372	1.8297	HOMO→LUMO (94%)
c60hr	920.8507	1.8023	HOMO→LUMO (94%)
c54hb	923.8699	0.3222	HOMO→LUMO (90%)
c74hr	928.7141	1.1620	HOMO→LUMO (93%)
c60ha	941.0500	0.3354	HOMO→LUMO (88%)
c50ha	942.9108	0.3294	HOMO→LUMO (89%)
c60he	959.4006	0.9232	HOMO→LUMO (92%)
c60hg	959.8462	0.6174	HOMO→LUMO (93%)
c54ha	975.8625	0.3409	HOMO→LUMO (88%)
c54hf	985.0110	0.9331	HOMO→LUMO (92%)
c74he	994.1732	1.0510	HOMO→LUMO (87%)
c58h32	1002.9391	0.3537	HOMO→LUMO (87%)
c74hd	1010.7063	1.0094	HOMO→LUMO (82%)
c74hc	1024.2324	0.3657	HOMO→LUMO (85%)
c62h34	1026.2672	0.3674	HOMO→LUMO (85%)
c66h36	1045.7434	0.3821	HOMO→LUMO (84%)
c74hb	1053.2054	0.3891	HOMO→LUMO (82%)
c70h38	1062.0467	0.3977	HOMO→LUMO (82%)
c60hc	1064.8745	1.0999	HOMO→LUMO (92%)
c74hg	1191.0023	1.1662	HOMO→LUMO (92%)
c60hd	1193.2949	0.9702	HOMO→LUMO (91%)
c74hf	1209.8296	1.2112	HOMO→LUMO (91%)
c74hh	1359.3174	1.0917	HOMO→LUMO (91%)
c74hi	1405.2288	0.9118	HOMO→LUMO (89%)
c74hw	1793.4809	1.0937	HOMO→LUMO (90%)
c74hz	1794.7790	1.1039	HOMO→LUMO (90%)

c74hy	1911.5531	1.0413	HOMO→LUMO (87%)
c74hx	1927.6016	1.0427	HOMO→LUMO (87%)
c33h15	1980.5645	0.0213	HOMO(B)→L+1(B) (61%), H-1(A)→LUMO(A) (13%)
c74hp	2049.6501	0.9875	HOMO→LUMO (84%)
c74ho	2068.8025	0.9320	HOMO→LUMO (84%)
c74hn	2104.2657	0.8585	HOMO→LUMO (83%)
c74hm	2176.2917	0.7512	HOMO→LUMO (83%), H-1→L+1 (10%)
c78h24	2427.7137	0.2894	HOMO→LUMO (14%), HOMO→L+1 (20%), H-1→LUMO (20%), H-1→L+1 (14%), H-1→L+2 (21%)
c28hcc	3158.0065	0.2001	HOMO→LUMO (87%)
c46h18	4221.4279	0.1481	HOMO→LUMO (50%), H-1→L+1 (36%)
c28hS	4251.8291	0.1646	HOMO→LUMO (86%)
c24h14c	4335.0817	0.0951	HOMO→LUMO (90%)
c24hc	4335.0817	0.0951	HOMO→LUMO (90%)
c32he	4359.4703	0.1278	HOMO→LUMO (90%)
c28hM	4413.7891	0.1169	HOMO→LUMO (88%)
c32hc	4659.2761	0.1125	HOMO→LUMO (90%)
c28hR	6156.0743	0.0708	HOMO→LUMO (89%)
c74hj	6515.1517	0.0958	HOMO→LUMO (58%), H-1→LUMO (34%)
c28hss	6687.3429	0.0515	HOMO→LUMO (91%)
c38hk	7505.0446	0.0535	HOMO→LUMO (89%)
c28hj	10818.7903	0.0297	HOMO→LUMO (92%)
c30hj	12167.1577	0.0236	HOMO→LUMO (92%)
c34hg	12251.3178	0.0284	HOMO→LUMO (92%)
c26hR	18126.2188	0.0137	HOMO→LUMO (93%)

**Table S2:** System names, wavelength corresponding to, oscillator strength (Osc. Str.) of and molecular orbital contributions for “ $p_{max}$  excitation” of all the GQDs whose  $p_{max}$  is in IR-region. Names of the GQDs are as given in Ref 23 of the main article. All the corresponding structures can be obtained from this link. [http://journals.aps.org/prb/supplemental/10.1103/PhysRevB.81.085430/GNFs\\_PAHs\\_coord.tar.gz](http://journals.aps.org/prb/supplemental/10.1103/PhysRevB.81.085430/GNFs_PAHs_coord.tar.gz)

**Table S3:** System names, wavelength corresponding to “ $p_{max}$ ” and “ $\beta_{max}$ ” excitations of all C28-GQDs whose  $p_{max}$  is in IR-region are given. Values inside the paranthesis are the ZINDO/S results and the ones which are outside are the CAM-B3LYP/6-31+g(d) results.

System	$p_{max}$ (nm)	$\beta_{max}$ (nm)
c28hcc	2966.1085 ( 3158.0065)	436.1311 (460.6820)
c28hj	4125.9014 (10818.7903)	346.5642 (429.1269)
c28hM	3035.8310 ( 4413.7891)	434.3282 (460.0666)
c28hR	3145.1887 ( 6156.0743)	393.7104 (454.2180)
c28hS	2896.1303 ( 4251.8291)	425.8401 (491.0231)
c28hss	3408.0082 ( 6687.3429)	397.7012 (448.3378)

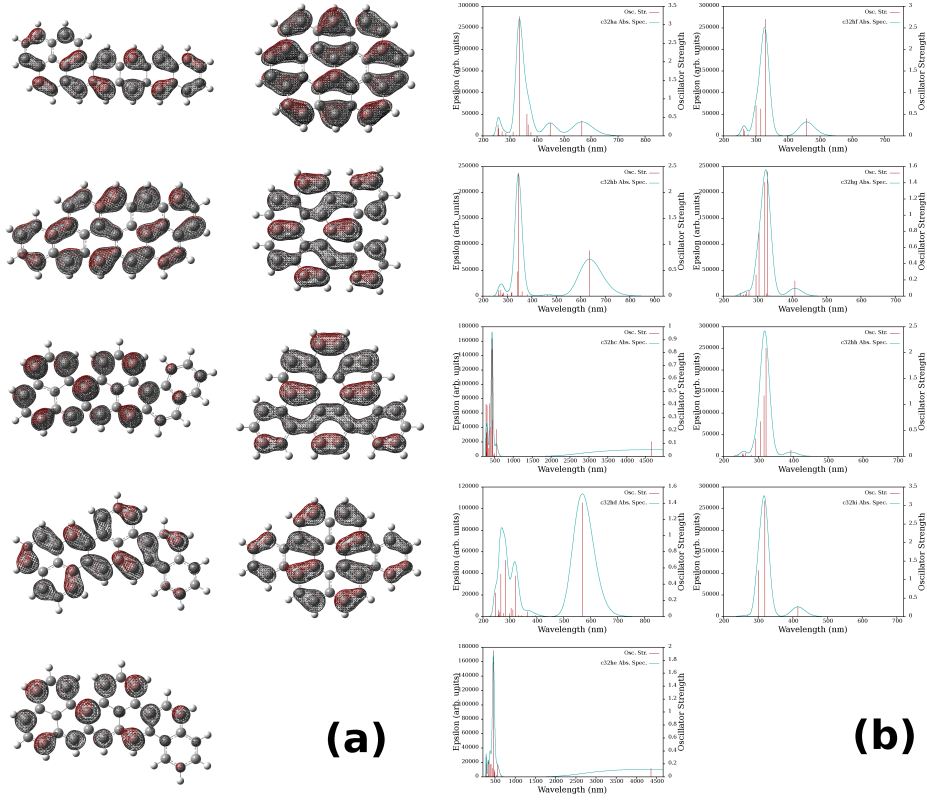


**Figure S2:** Panel (a) shows the isosurfaces of HOMO of all C32 GQDs considered in this study. Panel (b) shows their corresponding absorption spectra.

**Table S4:** System name, polarizability and 1st hyperpolarizability of C28-GQDs. Values inside the paranthesis are the MOPAC results and the outside ones are CAM-B3LYP/6-31+g(d) results.

System	$\alpha$ (a.u)	$\beta$ (a.u)
c28hcc	744.480 (1502.36167)	97762.095 (485305.1890)
c28hM	761.495 (1696.01550)	199892.814 (1304022.4046)
c28hss	801.149 (1726.62126)	437976.831 (2003517.2092)
c28hj	822.574 (2264.26242)	869985.316 (5567249.5402)

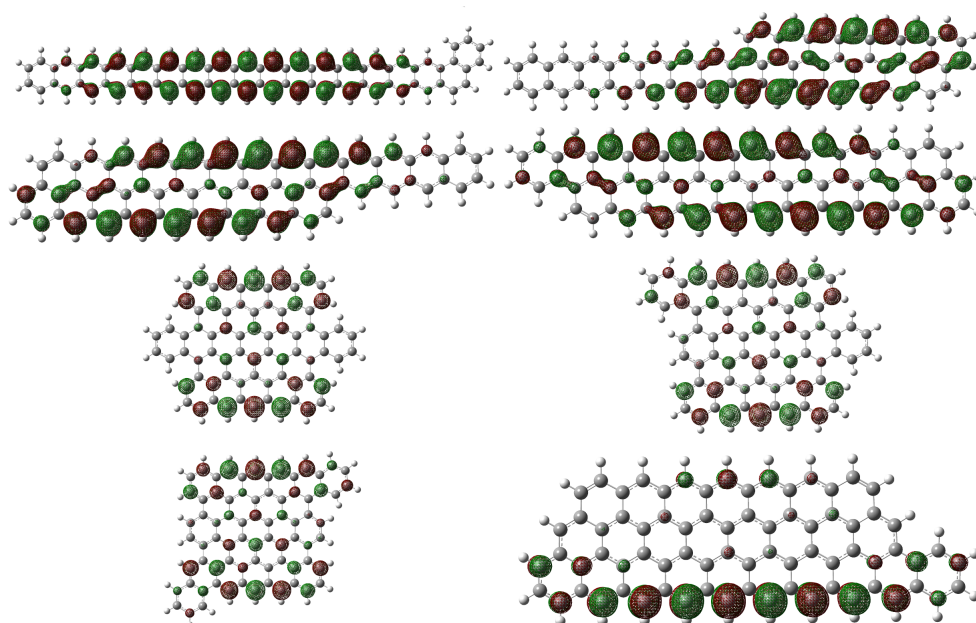


**Figure S3:** Isosurfaces of HOMO of some of the C74 GQDs considered in this study.

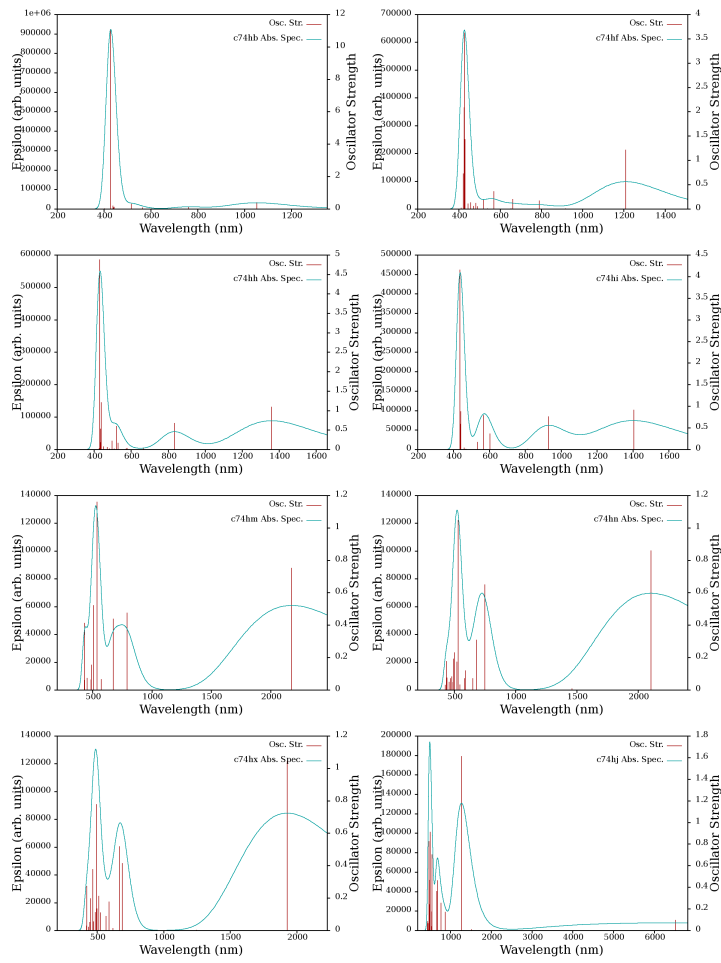


**Figure S4:** Absorption spectra corresponding to the QDs given in the above figure (Fig. S3).